J Appl Electrochem (2011) 41:1301–1309
DOI 10.1007/s10800-011-0345-5

ORIGINAL PAPER

Studies on the oxidation rate of metallic inert anodes by measuring the oxygen evolved in low-temperature aluminium electrolysis

V. A. Kovrov · A. P. Khramov · Yu. P. Zaikov · V. N. Nekrasov · M. V. Ananyev

Received: 20 June 2011 / Accepted: 13 August 2011 / Published online: 28 August 2011

Abstract The rate of oxygen evolution on metallic inert anodes was measured as a function of current density during electrolysis of a low-melting NaF(12)–KF–AlF_3 bath ($[NaF + KF]/[AlF_3] = 1.5$ mol mol^{-1}) at 800 °C. The oxidation rate of the anode substrate (A cm^{-2}) was calculated. The anode oxidation process was depressed at the potentials of oxygen evolution. The dynamics of the decrease in the oxidation rate, which were obtained in previous study by the change in geometrical size of the metallic part of the specimen, was reproduced both by the technique proposed and also in potentiostatic electrolysis at potentials below that of oxygen evolution, in some cases, depending on prepolarisation.

Keywords Molten salts · Aluminium electrolysis · Low-temperature electrolyte · Inert anode · Oxidation rate · Passivation

1 Introduction

The electrolysis of cryolite–alumina melts with an oxygen-evolving metallic anode is accompanied by intensive substrate oxidation. Consequently, the replacement of a carbon anode by an inert metallic anode has been unsuccessful. Low-melting systems based on KF instead of a conventional electrolyte decrease the working temperature by 100–150 °C. These systems could lead to substantially prolonged lifetimes of the anode because of the significant reduction of the oxidation rate [1–3]. Towards this end, we report here our investigation of the oxidation rate of metallic anodes in the course of low-temperature aluminium electrolysis.

The determination of the oxidation rate of metallic alloys, which are the best candidates for anode materials, was performed in an oxidising atmosphere [4–8] by gravimetry and in the course of aluminium electrolysis as anodes [1–3, 9, 10]. The general oxidation rate of the metal substrate can be estimated from the changes in the thickness of its metal (non-oxidised) part [1, 2, 9] and also from the metal oxidation current at potentials less than that required for oxygen evolution [9, 10]. These methods, however, exhibit some principal disadvantages.

The first method, which is supplemented with the analysis of the anode oxidation products and those dissolved in the melt, is considered to be the most exact method, but it requires long-term electrolysis tests, on the order of tens of hours [2], at a given current density. It does not allow the oxidation rate as a function of current density (or potential) to be determined in a single experiment. Such measurements require a series of long-term electrolysis tests.

Estimations of the oxidation rate from electrochemical responses ($E - i$ [9] and $i - \tau$ [10] curves) are easy to perform; however, these methods are inexact because they do not consider oxidation processes at potentials greater than that of oxygen evolution. In our opinion, the determination of the flow rate of oxygen evolved by the anode or of the oxygen concentration in the mixture with a gas carrier (as performed in [11]) could be very useful. The combination of this method with electrochemical measurements would provide a helpful alternative to the previously discussed methods. Such a method could allow the calculation of the anode oxidation rate (in units of current)

V. A. Kovrov (✉) · A. P. Khramov · Yu. P. Zaikov · V. N. Nekrasov · M. V. Ananyev
Institute of High Temperature Electrochemistry, S.Kovalevskoy, 22, Ekaterinburg, Russia 620219
e-mail: kovrov@ihte.uran.ru

as the difference between the total current and the current responsible for the discharge of oxygen that has left the reaction interface.

The aim of the present study is to implement the previously mentioned investigation techniques, coupled with measurements of the oxygen generated during electrolysis. As an example, experimental data for a Cu–Al, Cu–Ni–Fe and Cu–Ni–Fe–Al alloys, which have been previously investigated as anodes [1–3, 5, 7, 11], are given. Furthermore, the applicability of the proposed methods is demonstrated. The possibilities and limitations of the oxidation-rate study based on oxygen flow rate, determined together with electrochemical measurements, are also discussed.

2 Experimental

2.1 Cell

Experiments were performed in a three-electrode open cell depicted in Fig. 1. An alumina crucible ($h = 120$ mm, $d = 80$ mm) containing the electrolyte was placed into the container made of refractory steel. The space between the crucible and the container was impounded with finely dispersed graphite.

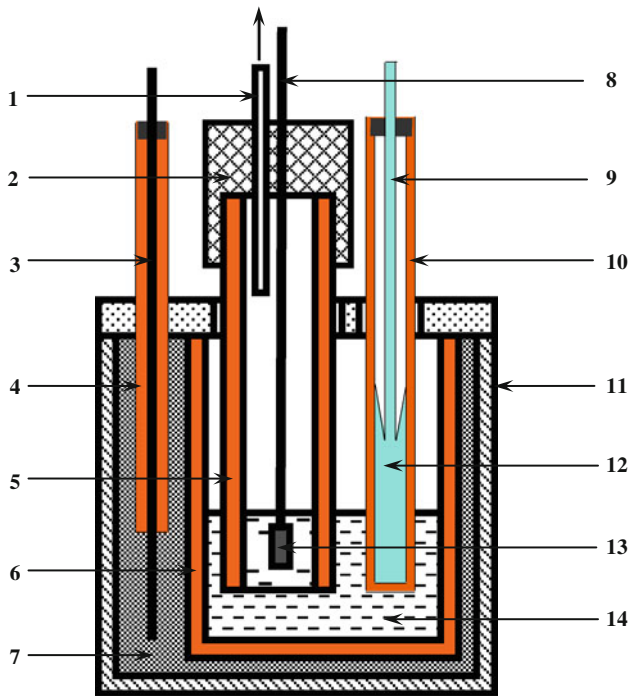

Fig. 1 Scheme of the open experimental cell for the anode gas collection during electrolysis: *1* outlet pipe for anode gas (connected with the capillary of the rheometer); *2* rubber stopper; *3* cathode current lead (nichrome or *W*); *4*, *5* alumina tubes; *6* sintered alumina crucible; *7* cathode (finely dispersed graphite); *8* anode current lead (Pt); *9* Al wire; *10* porous alumina sleeve; *11* refractory steel container; *12* Al in the reference electrode; *13* anode; *14* electrolyte

2.2 Chemicals and bath preparation

The melt composition was NaF(12)–KF–AlF_3 (wt%) with cryolite ratio (CR) of 1.5 (CR = ([KF] + [NaF])/[AlF_3], mol mol^{-1}). The individual salts NaF, AlF_3 and alumina were of technical grade and were used for the bath preparation. Reagent KF was prepared by thermal decomposition of KF·HF by gradually heating the adduct to 850 °C for 5 h. The components were mixed and melted, and an amount of alumina that corresponded to saturation (6.5 wt%) was added with stirring. The temperature was maintained 20 °C above the melting point during the experiments, i.e. 800 °C. The alumina solubility and the liquidus temperature have been reported elsewhere [12, 13]. The temperature was monitored during the experiments using a Pt–PtRh thermocouple in a sintered alumina sleeve immersed in the electrolyte.

2.3 Electrodes

To collect gaseous products, the anode was shielded by a gas-tight tube made of sintered alumina, as shown in Fig. 1. The tube exhibited a diameter of 30 mm and a wall thickness of 3.5 mm. The upper part of the tube was sealed with a rubber stopper. The last has two holes accommodated the vent pipe and anode rod. The bottom parts of the tube and the anode sample were immersed in the melt. The distance between the anode and the tube butt-ends in the vertical direction was maintained at a minimum of 5 mm; this spacing allowed the collection of the gas bubbles within the tube and did not hinder mass transfer in the electrolyte between the anode surface layer and the bulk.

The anode sample was a cylinder ($d = 6$ mm, $h = 10$–11 mm). A Pt wire ($d = 1$ mm) was inserted into the anode as a current lead. The anode assembly was dipped into the electrolyte at a depth of 12–16 mm according to the anode working area, which varied from 2.5 to 2.6 cm^2. Hence, a so-called immersed anode was constructed. The immersed part of the Pt wire did not exceed 3–5% of the total working area. The compositions of the tested alloy anodes are given in Table 1. To avoid unaccounted oxidation, the anode sample was heated to the

Table 1 Composition of the alloy anodes tested

No.	Composition (wt%)
1	Cu–Al(3)
2	Cu–Ni(22)–Fe(30)
3	Cu–Ni(5)–Fe(5)–Al(8)
4	Cu–Ni(12)–Fe(23)

working temperature by immersion in the molten electrolyte.

Finely dispersed graphite powder placed between the outer steel container and the alumina crucible was used as the cathode. A porous crucible impregnated with electrolyte exhibited good electrical conductivity. No aluminium metal was placed in the electrolyte during electrolysis. Tungsten or nichrome rod was used as the current lead to the graphite cathode.

Potentials were measured with respect to the Al reference electrode with aluminium wire as the current lead [14].

2.4 Techniques and equipment

Three electrochemical techniques were used. Steady-state current versus potential curves were recorded point-by-point, and short electrolysis tests were performed both in galvanostatic mode with the measurement of oxygen. Short-term electrolysis at a fixed potential close to that of oxygen evolution was also performed (chronoamperometry).

Anode potentials during galvanostatic electrolysis were measured using a pulsed galvanostat after 5 μs of current interruption to determine the ohmic voltage drop (IR) in the electrolyte. Chronoamperometry was performed using an Autolab PGSTAT302 potentiostat (*EcoChemie*, Netherlands) controlled by GPES software.

2.5 Determination of the anodic gas flow rate

The effect of the rate of gas flow on the pressure drop at the capillary was determined using a U-tube manometer filled with dibutylphthalate. The pressure difference at the capillary was indicated by the difference in the levels between the two columns of the liquid. To change the limit of the flow meter, capillaries of different lengths were used. The flow meter was calibrated by passing a fixed quantity of gas (Ar, O_2) through the capillary within a certain period. Experimental points were approximated by a linear function according to the best fit. Maximum deviation of the experimental values of gas flow rate from the approximation function ($_{\Delta}V_{GAS}$, mL min^{-1}) and corresponding values $_{\Delta}i_{O_2}$ (A cm^{-2}) are given in Table 2.

To increase the accuracy, the internal volume of the anode shielded tube and the appropriate pipeline were filled with oxygen, and the argon-carrier pipeline was filled with argon. If the hydrodynamic resistance of the capillary is excessive, electrolyte would be displaced from the anode shielded tube by gas. The electrolyte displacing was accompanied by a drastic increase in the anode potential and its oscillations. To maintain the electrolyte within the tube at a constant level, the proper capillary was selected for the corresponding interval of current density.

2.6 Anodic gas analysis

Anodic gas was analysed by Agilent 5973N quadrupole mass spectrometer with electron impact ionization. For this purpose, electrolysis experiments with the argon as gas carrier were performed. Only the argon flow rate was measured in this type of experiment and the flow was maintained at an approximately constant rate when different current densities were applied. The argon was mixed with the anodic gas evolved during electrolysis and the mixture was then passed through the quartz vessel (35 mL) used as a gas sample container. The quartz vessel contained an outlet that slightly limited the flow. Approximately 150 mL of the gas mixture was removed from the vessel during the sampling. The initial atmosphere in the vessel was air.

3 Results and discussion

3.1 Experiments with gas carrier

Assuming that oxygen discharge is the only process on the anode:

$$2O^{2-} - 4e^{-} \rightarrow O_{2(g)}, \quad (1)$$

Then, oxygen concentration in the gas mixture (with argon) can be calculated as follows:

Table 2 The maximum deviation of the experimental values of gas flow rate from the approximate linear function

No.	Gas	Gas flow rate interval (mL min^{-1})	$\pm_{\Delta}V_{GAS}$ (mL min^{-1})	Interval of i_{O_2} [a] (A cm^{-2})	$\pm_{\Delta}i_{O_2}$ [a] (A cm^{-2})
1	O_2	0.08–1	±0.06	0.008–0.10	±0.006
2		1–5	±0.11	0.10–0.52	±0.011
3		5–10	±0.43	0.52–1.03	±0.045
4		10–25	±0.90	1.03–2.58	±0.093
5	Ar	0–3	±0.11		
6		3–10	±0.18		

[a] Calculated according to an anode working area of 2.5 cm^2

$$[O_2]_{outlet} = \frac{V_{O_2}}{V_{O_2} + V_{Ar}},$$

where $[O_2]_{outlet}$ is the oxygen concentration in the gas mixture at the outlet in mol mol^{-1}, V_{O_2} and V_{Ar} is the flow rates for oxygen and argon, respectively, in mL min^{-1}.

The technical-grade argon used as the gas carrier contains admixtures (Table 3), including oxygen. Therefore, the total oxygen flow rate V_{O_2} was calculated as the sum of the flow rate generated by the anodic reaction (1) and that of argon:

$$[O_2]_{outlet} = \frac{V_{O_2(anode)} + V_{O_2(Ar\ techn)}}{V_{O_2(anode)} + V_{Ar\ techn}}, \quad (2)$$

$$V_{O_2(anode)} = k \cdot I \cdot \beta_{(1)}, \quad k = 9,695 \cdot \frac{T}{p}, \quad (3)$$

$$V_{O_2(Ar\ techn)} = [O_2]_{Ar\ techn} \cdot V_{Ar\ techn}, \quad (4)$$

where $V_{O_2(anode)}$ is the oxygen flow rate generated by the anodic reaction (1); $V_{O_2(Ar\ techn)}$ is the oxygen flow rate added with technical-grade argon as an admixture; $V_{Ar\ techn}$ is the flow rate of the technical-grade argon; k is the electrochemical equivalent for O_2 evolved by reaction (1) in mL A^{-1} min^{-1}; I is the current in A; $\beta_{(1)}$ is the current efficiency of the reaction (1), fraction per unit; $[O_2]_{Ar\ techn}$ is the concentration of O_2 in the technical-grade argon in mol mol^{-1}.

The increase in the current load led to an increase in the oxygen concentration in the two-component gas mixture. The theoretical ($[O_2]_{outlet}$) and experimental (analysed) oxygen concentrations are given in Table 3. The first was provided by the assumption that $[O_2]_{outlet}$ is constant during the course of electrolysis and $\beta_{(1)} = 1$. A good correlation was observed between both concentrations, but the experimental concentrations were lower than expected. A reasonable explanation is that the O_2–Ar mixture was diluted by the air. As evident from Table 3, the difference between the $[O_2]_{outlet}$ and the experimental oxygen concentrations for the Pt anode and a Cu–Ni–Fe alloy were almost the same. This fact makes it impossible to calculate the oxidation rate of the alloy exactly.

3.2 Direct measurement of anodic oxygen

The current of reaction (1) can be expressed according to (3):

$$I_{O_2} = I \cdot \beta_{(1)} = \frac{V_{O_2(anode)}}{k}, \quad i_{O_2} = \frac{I_{O_2}}{S_a}, \quad (5)$$

where S_a is the anode working area in cm^{-2}. Equation 5 gives the oxidation current of the oxygen that has left the reaction zone, I_{O_2} (A) and i_{O_2} (A cm^{-2}). The use of Eq. 5 is appropriate when only the oxygen flow rate from the anode ($V_{O_2(anode)}$) is determined. No gas carrier was used and the flow meter was directly connected to the anodic gas pipe. This approach is interesting with respect to the metal anode being partially oxidised; calculations of oxidation rate can then be realised using experimentally determined $V_{O_2(anode)}$.

The polarisation curve for the Pt anode obtained in galvanostatic mode at a steady-state condition is presented in Fig. 2. The oxygen current i_{O_2}, which was calculated from experimental values of $V_{O_2(anode)}$ using Eq. 5, is also shown. The dotted line marks the potential of the initial oxygen evolution registered by the technique. Figure 2 also exhibits a difference between the current i (A cm^{-2}) and the calculated values of i_{O_2}. These two values clearly tend to be equal in the case of an inert anode and $\beta_{(1)} = 1$. The maximum deviation observed for the Pt anode does not exceed 5% of the i_{O_2} values.

Table 3 Composition of the gas mixture O_2–Ar obtained by mass-spectrometric analysis and theoretical O_2 concentrations for experiments with different current loads

No.	I, A (i, A cm^{-2})	Ar techn. flow ($V_{Ar\ techn}$) (mL min^{-1})	O_2–Ar mixture composition, mol%					
			Analysed					Calculated
			CO_2	Ne	N_2	Ar	O_2	$[O_2]_{outlet}$
1[a]	1.0 (0.4)	5.00	0.3	4.3	6.1	48.4	40.9	43.9
2	1.0 (0.5)	5.03		4.5	5.2	51.2	38.8	44.2
3	2.0 (1.0)	4.91		3.0	3.7	35.0	58.0	62.0
4	3.0 (1.5)	5.08		2.5	2.9	28.8	65.5	70.1

Electrolyte composition, wt%: NaF(12.0)–KF(36.8)–AlF_3(51.2); CR = 1.5; T = 800 °C; anode Pt

Technical grade Ar composition, mol%: Ne, 8.3; N_2, 2.5; Ar, 88.2; O_2, 1.0

Electrolyte was composed by mixing KF·HF with other components, followed by gradually heating for 7 h up to the working temperature

[a] Anode metallic alloy No 4, Table 1

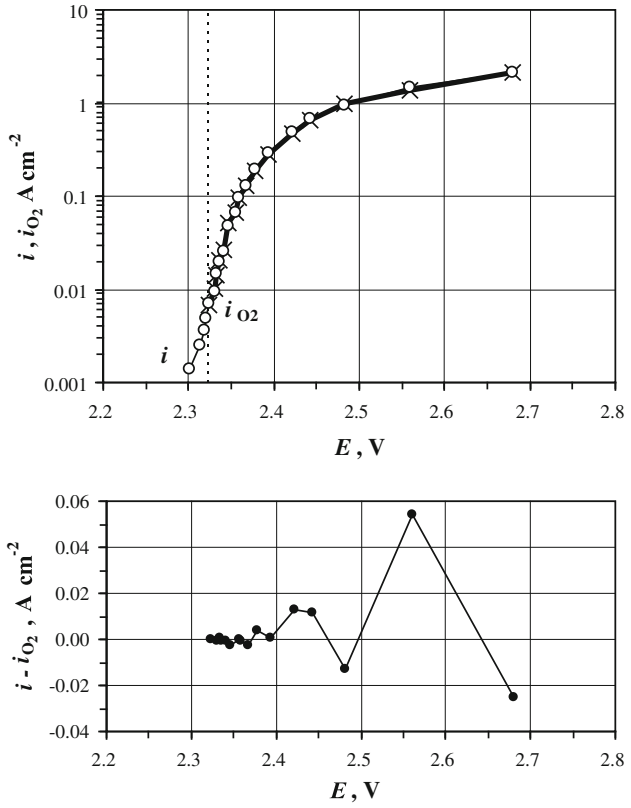

Fig. 2 Current density (*open circle*) versus anode potential curves with respect to Al reference electrode; oxygen current, i_{O_2} (*times symbol*). The difference between i and i_{O_2} values (5). Anode *Pt*

3.2.1 *Calculation of the anode oxidation rate during electrolysis*

As previously mentioned, a calculation of i_{O_2} that is based on the experimental oxygen flow rate is of interest when anodes are partially oxidised during electrolysis ($\beta_{(1)} < 1$). The oxidation rate i_{OX} (A cm^{-2}) can be calculated as follows:

$$i_{OX} = i - i_{O_2}, \quad i = I/S_a, \tag{6}$$

The anode oxidation rate obtained from Eq. 6 comprises a number of oxidation processes taking place on the metallic anode, including all of the electrochemical reactions of the anode-component's oxidation (processes accompanied by charge transfer):

$$M_{(s)} + xF^- - xe^- \rightarrow (MF_x)_{(diss)}, \tag{7}$$

$$M_{(s)} + x/2O^{2-}_{(diss)} - xe^- \rightarrow (MO_{x/2})_{(s)}, \tag{8}$$

$$M_{(s)} + \frac{4+x}{2}O^{2-}_{(diss)} - (4+x)e^- \rightarrow (MO_{x/2})_{(s)} + O_{2(g)}, \tag{9}$$

where x is the oxidation number of metal M, $O^{2-}_{(diss)}$ is oxygen in the form of dissolved oxy-fluor aluminate complex, $(MO_{x/2})_{(s)}$ is solid oxide. Furthermore, the anode oxidation involves the series of consecutive reactions that consist of the electrochemical stage (1), as well as the chemical reactions with participation of oxygen as the intermediate oxidation product. In other words, reaction (1) produces an amount of oxygen that chemically oxidises an anode substrate.

The value of i_{OX} is considered the oxidation rate of an anode. Significant differences between this value and the real value could only be observed if the current leads or the upper part of a metallic anode that is not immersed in electrolyte are exposed to be oxidised by gaseous oxygen [11]. The current leads must therefore be protected by a gas-tight shield or made of Pt.

Figure 3 presents the steady-state current i_{O_2} and i_{OX} (calculated by Eqs. 5, 6) versus potential curves for the alloy anodes under investigation; the values were obtained by the same method used for the Pt anode. In most cases, the time necessary to stabilise the oxygen flow and the potential of the anode was about 2 min for each applied current density. Some points at the potentials of oxygen evolution were stabilised for up to 15 min.

The significant 'lack' of oxygen compared to 100% efficiency for reaction (1) was observed in experiments with the alloy anodes. The difference between the applied current density i and i_{O_2}, which was calculated on the basis of experimental $V_{O_2(anode)}$, was greater than 50% in the region of the potentials that were close to those of oxygen evolution. This difference significantly exceeds the error of the i_{O_2} that was determined as shown for the case of the Pt anode. These results indicate that the intensive process of the anode substrate oxidation occurs.

A noticeable decrease of the alloy-anode oxidation rate at the potential of intensive oxygen evolution (1), i.e. at the moment when the gas evolution starts (standard EMF of alumina decomposition, $E_{800^\circ C}$: 2.3 V [15], 2.31 V [16]). The decrease in the oxygen rate was not related to any errors in the measurements: the decrease in i_{OX} was significantly greater than 5% compared to the maximum value of i_{O_2} at the potentials were i_{OX} decreased. The process of the molecular oxygen generation was possibly preceded by the formation of a relatively high concentration of the chemisorbed oxygen, which led to the noticeable passivation of the active electrode surface.

As was previously mentioned, the stabilisation time for each point of the steady-state $i - E$ curve was 2–5 min; however, the first point of initial oxygen evolution was stabilised for 10–15 min. The potential shifts for a few minutes. As it reaches the oxygen potential, the electrolysis process occurs at a relatively constant potential, and only afterwards does the rheometer begin to register the first portion of oxygen. The formation of gaseous oxygen was

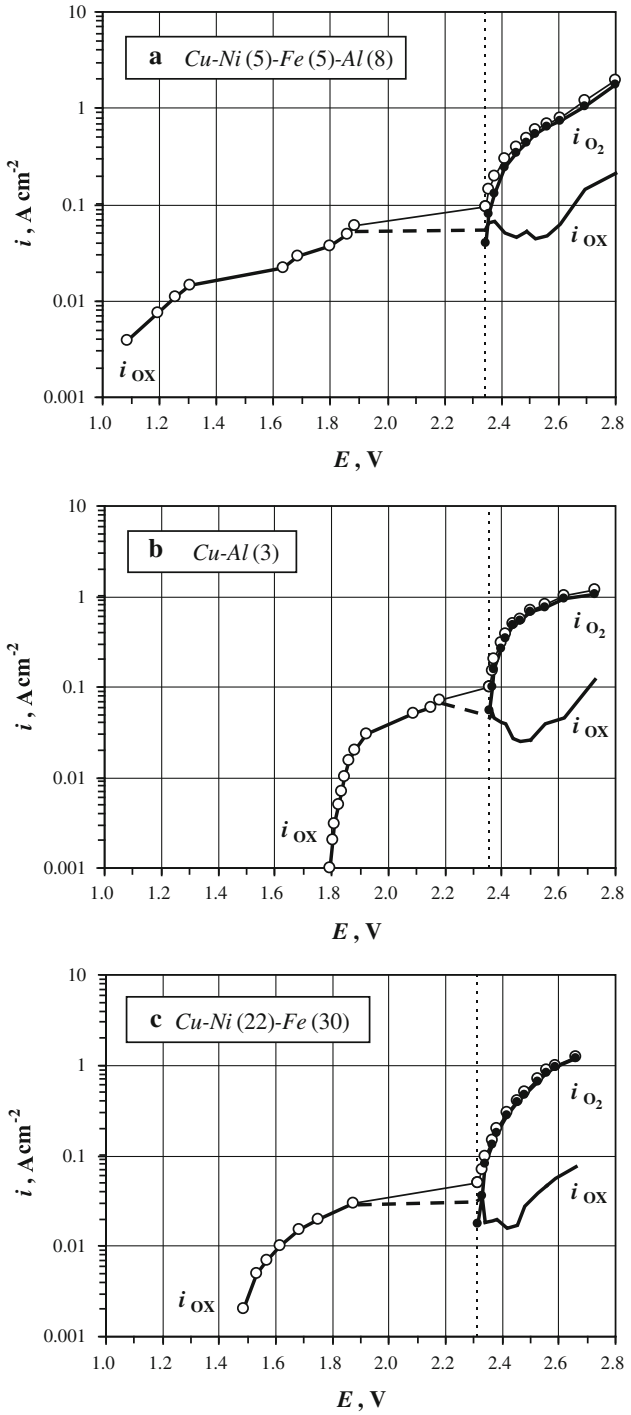

Fig. 3 Current density, i (*open circle*) and oxygen-evolving current, i_{O_2} (*filled circle*) versus potential curves for anodes, wt%: **a** Cu–Ni(5)–Fe(5)–Al(8); **b** Cu–Al(3); **c** Cu–Ni(22)–Fe(30); S_a = 2.5–2.6 cm^2. Open-circuit potential (**a**, **b**, **c**), V: 0.99, 1.79, 1.48 with respect to Al reference electrode

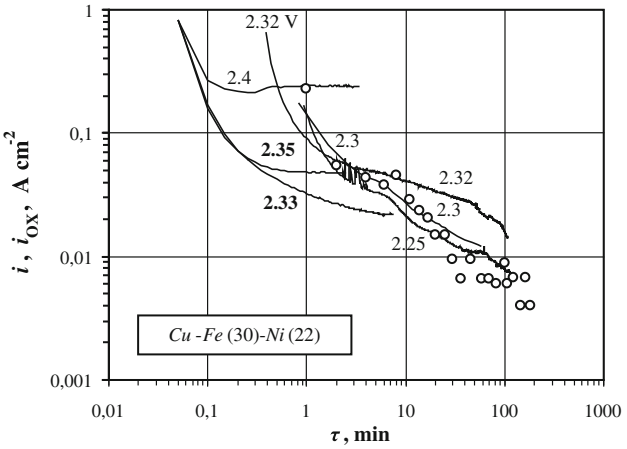

Fig. 4 Potentiostatic polarisation of the alloy anode, wt%: Cu–Ni(22)–Fe(30); previously oxidised samples: 2.35 and 2.33 V. The charge in the period of the potential setting ($\tau_{initial}$), Coulombs cm^{-2} (s): 2.25 B − 13 (56), 2.3 B − 12 (50), 2.32 B − 8.2 (23), 2.4 B − 2.5 (3), 2.35 B − 2.5 (3), 2.33 B − 2.5 (3). The variation of the i_{OX} with time (*open circle*): calculated by (6) for galvanostatic polarisation, i = 0.43 A cm^{-2}

probably related to the 'increase of oxidisability' of the anode surface, and the partial or complete oxidation of the metal anode surface is followed by the evolution of gas.

The evolution of the current density with time during the potentiostatic polarisation of the alloy anodes at potentials below that of oxygen evolution, Figs. 4, 5 and 6, can be interpreted from this point of view. When observing the chronoamperometric curves, the lack of immediate potential stabilisation due to the current limitation (2 A) of the galvanostat must be considered; it was shifted from stationary to the given value through some intermediate steps. In the case of sample 2 (Table 1), we attempted, where possible, to shorten the period required to establish the potential; this period is not represented in Fig. 4. The initial part of the curves corresponds to the moment where the given potential was set; this time is represented by $\tau_{initial}$ (see figure legend). Anodes used in chronoamperometry tests were halfway immersed, with the exception of the run at 2.3 V (immersed, Pt current lead, Fig. 4). For the last case, the measurement of $V_{O_2(anode)}$ was also performed, and no oxygen was registered at the cell outlet. Therefore, at least at potentials more negative than 2.3 V, the observed currents are due only to the oxidation of the anodes.

The anode surface was renewed after each polarisation run or when a new sample of the same composition was tested; the curves at 2.35 and 2.33 V were not renewed (Fig. 4). Points i_{OX}, which were calculated on the basis of $V_{O_2(anode)}$ (5) in the galvanostatic experiments at the potentials above oxygen evolution, are also plotted. As evident from Fig. 4, a relatively large amount of charge is necessary (figure legend) to establish the potential that is not sufficiently positive for the evolution of oxygen. The oxidation probably proceeded deep into the anode substrate without passivation for a relatively long time at this

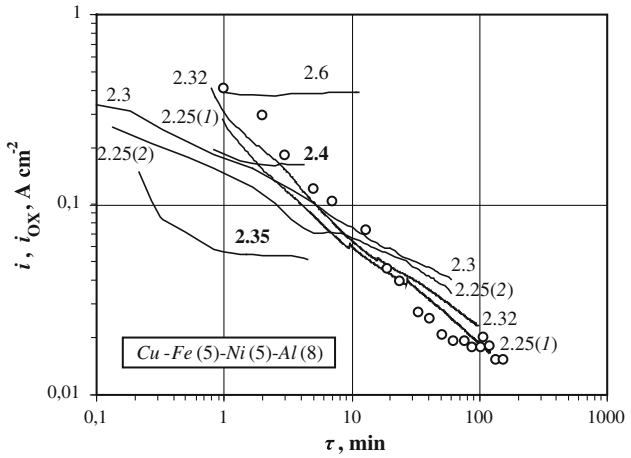

Fig. 5 Potentiostatic polarisation of the alloy anode, wt%: Cu–Ni(5)–Fe(5)–Al(8); previously oxidised samples: 2.4 and 2.35 V. The charge in the period of the potential setting ($\tau_{initial}$), Coulombs cm^{-2}, s: 2.25 B (1) − 13 (58), 2.32 B − 8.4 (48), 2.25 B (2) − 9 (8), 2.3 B − 6 (1), 2.35 B − 0.8 (13), 2.4 B − 7 (50), 2.6 B − 7 (60). The variation of the i_{OX} with time (*open circle*): calculated by (6) for galvanostatic polarisation, $i = 0.44$ A cm^{-2}

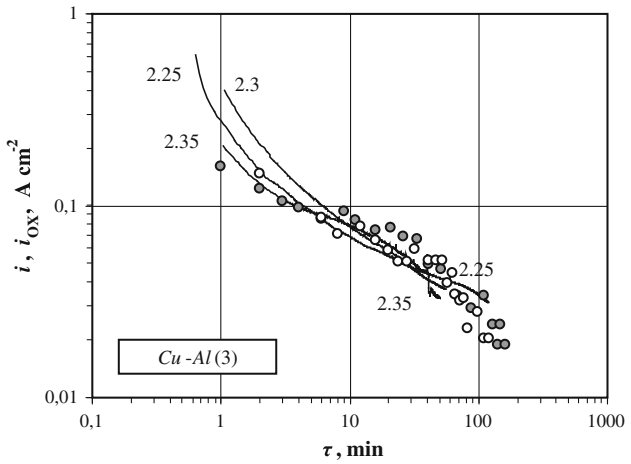

Fig. 6 Potentiostatic polarisation of the alloy anode, wt%: Cu–Al(3). The charge in the period of the potential setting ($\tau_{initial}$), Coulombs cm^{-2} (s): 2.25 B − 8 (38), 2.3 B − 17 (64), 2.35 B − 18 (63). The variation of the i_{OX} with time (*open circle*, *filled circle*): calculated by (6) for galvanostatic polarisation, $i = 0.41$ (*filled circle*), 0.40 (*open circle*) A cm^{-2}

potential. We assume that a sufficient increase in the degree of surface oxidation is not immediately achieved, because the atomic chemisorbed oxygen has time to 'drain' deep into the substrate, and the relatively low concentration at the surface remains.

The situation changed with the application of a sufficiently high potential. The concentration of oxygen on the surface increases to the point at which a significant passivation, i.e. a sufficient increase in the degree of surface oxidation, does not require a large amount of electricity. Figure 4 shows that a sufficiently high potential can be considered as 2.33 V and above. At that point, the character of the curve begins to change: as passivation is in progress, a decrease is observed in the rate of the total current decrease. This is particularly evident for the curve at 2.4 V: after rapid passivation, the current of oxygen discharge i_{O_2} increases, whereas the current of the anode oxidation i_{OX} is probably decreased (possibly at the same rate as for the galvanostatic experiment–points in the figure) so that the total current remains constant.

At the initial stage of electrolysis, the rate of oxidation strongly depends on the degree of surface passivation, i.e. prepolarisation. This is clearly seen when comparing the curves at 2.32 and 2.33 V. In the latter case, i_{OX} is noticeably lower. From this perspective, the i_{OX} component (the curve at 2.4 V) is much lower than the points in the figure, and the total current largely consists of i_{O_2}.

The chronoamperometric curves were also obtained for other alloys, Fig. 5, 6. In these cases, we did not seek to reduce the period required to establish the potential. The curves at 2.4 and 2.35 V in Fig. 5 were obtained for the anodes without the oxide layers removed. The previously mentioned dependence of the oxidation rate on the degree of surface passivation is observed only at the initial stage, and after some time (probably on the order of hundreds of minutes), the oxidation rate becomes constant, independent of the initial passivation.

The polarisation curves presented in Fig. 3 could be considered stationary only in conditional terms. The anode is oxidised continuously, and the speed of this process continuously decreases with increasing thickness of the oxide layer. Accordingly, in a galvanostatic experiment, the potential is continuously shifted in the positive direction at a given current density. For measurements at potentials where the rapid release of oxygen occurs, the oxygen current is much greater than the current of the substrate oxidation ($i_{O_2} \gg i_{OX}$). This curve consequently varies much more slowly.

The galvanostatic electrolysis was performed with the alloy anodes at potentials greater than that of oxygen evolution. The anode potential was varied from 2.4 to 2.55 V, and the oxygen flow rate noticeably increased with time. Based on calculations by (5), (6), the variation of the anode oxidation rate with time, $i_{OX} - \tau$, can be obtained, Figs. 4, 5 and 6 (points). For all cases, the dynamics of the anode's oxidation rate in the galvanostatic experiments at the potentials of oxygen evolution are almost the same as those observed in potentiostatic electrolysis without gassing at potentials below the point of oxygen evolution. The $i_{OX} - \tau$ data can be compared with that presented in a previous article, which were obtained from the changes of the thickness of the metallic (nonoxidised) part of the alloy anode in a series of long-term electrolysis tests (3–72 h) [2].

To compare the oxidation rates obtained by two methods, i_{OX} (A cm^{-2}) must be transformed to V_{OX} (cm year^{-1}):

$$V_{OX} = \left(\frac{A}{zF}\right)_{average} \cdot \frac{\tau}{\rho} \cdot i_{OX} = \frac{326.8}{\rho}\left(\frac{A}{z}\right)_{average} \cdot i_{OX}, \quad (10)$$

where $\left(\frac{A}{zF}\right)_{average}$ is the average electrochemical equivalent for alloy under oxidation, A in g mol^{-1}, F in A h mol^{-1}, τ in h year^{-1}, i_{OX} in A cm^{-2}, and ρ is the alloy density in g cm^{-3} (to yield a more exact result, ρ could be determined as the density of the alloy with the composition obtained from both oxide scale and the anode components dissolved in electrolyte after its complete chemical reduction). The oxidation number of the alloy components for the calculation $\left(\frac{A}{z}\right)_{average}$ must be determined:

$$\left(\frac{A}{z}\right)_{average} = \sum \left(\frac{c_i A_i}{z_i}\right) \cdot \frac{1}{100} \quad (11)$$

where c_i is the concentration of the oxidised alloy component in at.%, z_i is the oxidised alloy component's oxidation number. To perform a correct calculation, it must be taken into account that alloy components dissolve from the oxide scale somewhat selectively, and the component ratio hence differs from that in the substrate alloy. The ratio of the same component with different oxidation numbers also changes during long-term oxidation. Therefore, the results of such calculations (11) will yield an evaluative result. To enhance the calculation accuracy, results of the oxide-layer X-ray phase analysis or experimental data on the oxide-layer phase structure can be used. Figure 7 depicts the evolution of the oxidation rate in units of cm year^{-1} with time, plotted on a logarithmic scale, for the Cu-based anodes. Here, V_{OX} (cm year^{-1}) was calculated on the basis of the c_i and ρ of the substrate alloy.

Satisfactory agreement is observed between the data on the oxidation rate V_{OX} (cm year^{-1}) for the alloy wt%: Cu–Ni(5)–Fe(5)–Al(8) based on the oxygen measurement in short-term electrolysis tests and that presented in a previous article [2]. The best fitting of the data presented in Fig. 7a is provided for $z_{Cu} = 0.7$ (Cu–Ni(5)–Fe(5)–Al(8)) and $z_{Cu} = 2$ for Cu–Al(3) in Fig. 7b.

The accuracy of the technique applied for the evaluation of the oxidation rate is an important parameter. Because it is a major material characteristic (V_{OX} or i_{OX}), the alloy that exhibits the lowest oxidation rate is of greater interest. Furthermore, V_{OX} decreases with time at a relatively high rate for all of the tested alloys, Figs. 4, 5 and 6, [2]. The method that exhibits greater accuracy would provide a long-lasting control of the oxidation process and a reasonable forecast of further decreases in the oxidation rate. The methodic limitation in this case is the determination of a small deflection of the anodic gas flow rate against a relatively large background. The test sensitivity (a) could

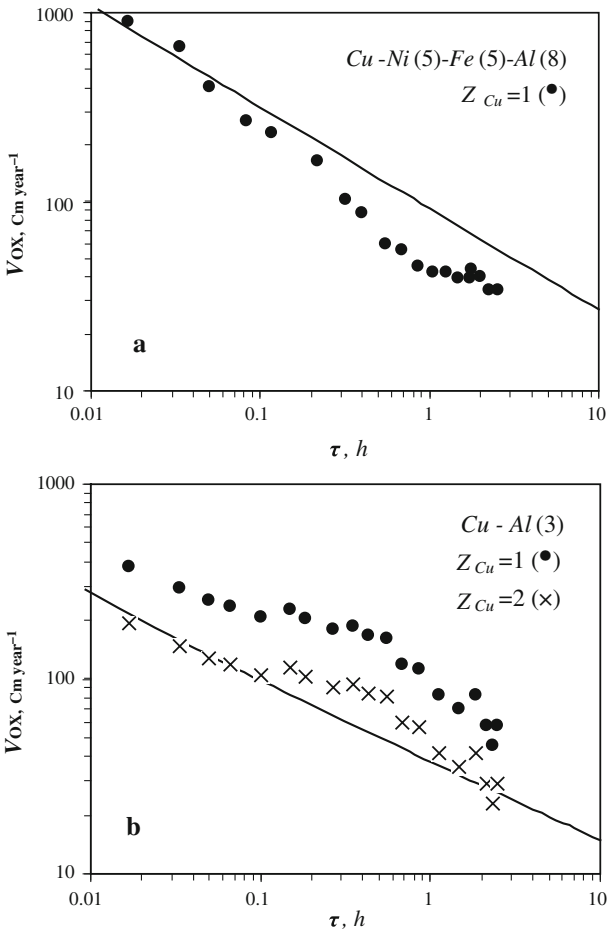

Fig. 7 The evolution of the oxidation rate, V_{OX} (cm year^{-1}) with time during galvanostatic polarisation for the anodes, wt%: **a** Cu–Ni(5)–Fe(5)–Al(8), $i = 0.44$ A cm^{-2}, $I = 1.1$ A; **b** Cu–Al(3), $i = 0.41$ A cm^{-2}, $I = 1.0$ A. Calculated from the Eqs. 5, 6, 10, 11 on the basis of $z_{Cu} = 1$ (*filled circle*), $z_{Cu} = 2$ (*times symbol*). *Line* indicates the extrapolated part of the $V_{OX} - \tau$ curve obtained by the changes in the geometrical sizes of the metallic part of the alloy anode in a series of long-term electrolysis tests (3–72 h, $T = 790$ °C) [2]

be evaluated as the maximum ratio of current load and the alloy oxidation current:

$$a = \frac{i}{(i - i_{O_2})_{min}} = \frac{i}{i_{OX\,min}} \quad (12)$$

where i_{OXmin} is minimal determining oxidation rate at the given i. In the previously described cases of current densities of $i = 0.1$–0.44 A cm^{-2}, the value i_{OXmin} was 0.019–0.015 (i.e. 4.5–3.5% from i). The lowest determined oxidation rate, V_{OX}, was 35–25 cm year^{-1}. Hence, the proposed method exhibits a maximal test sensitivity of $a = 22$–28.

4 Conclusions

We believe the investigations reported here, which were obtained with an exact measurement of the oxygen flow

rate, are of interest for the correct determination of alloy anode oxidation rates in the electrolysis of aluminium and for the further investigation of the oxidation kinetics. Such data would be helpful when choosing the regime of electrolysis (potential or current density) for the sake of prolonging the anode lifetime. The dynamics of the oxidation rate exhibit a single value for the passivation properties of the oxide films; hence, the technique proposed could be considered as an evaluative test of film stability. Periodic measurements of oxygen during long-term (tens of hours) tests is especially interesting; however, such measurements would require a significant (an order of magnitude) increase of the test's accuracy.

Acknowledgements This study was financially supported by the Program of the Ural Division of the Russian Academy of Sciences. The authors thank V. M. Chumarev for providing the alloys.

References

1. Kovrov VA, Khramov AP, Redkin AA, Zaikov YP (2008) Oxygen evolving anodes for aluminum electrolysis. In: Electrodes for Industrial Electrochemistry—214th ECS Meeting, Honolulu, HI, United States, 12–17 October 2008
2. Kovrov VA, Khramov AP, Shurov NI, Zaikov Yu P (2010) Russ J Electrochem (Engl Transl) 46(6):665–670
3. Beck TR, MacRae CM, Wilson NC (2011) Metal anode performance in low-temperature electrolytes for aluminum production. Metall Mater Trans B. doi:10.1007/s11663-011-9511-8
4. Sekhar JA, Liu J, Deng H et al (1998) Graded non-consumable anode materials. In: Welch B (ed) Light metals. TMS, Warrendale, pp 597–603
5. Shi Z, Xu J, Qiu Z et al (2003) JOM J Min Met Mater 55:63–65
6. Shi Z, Zhao X, Xu J et al (2008) Anti-oxidation properties of iron-nickel alloys at 800–900 °C. In: DeYoung DH (ed) Light metals. TMS, Warrendale, pp 1051–1054
7. Helle S, Davis B, Guay D, Roue L (2010) J Electrochem Soc 157:E173–E179
8. Chapman V et al (2011) High temperature oxidation behaviour of Ni–Fe–Co anodes for aluminium electrolysis. Corros Sci. doi:10.1016/j.corsci.2011.05.018
9. Filatov AY, Antipov EV, Borzenko MI et al (2008) Protect Metals (Engl Transl) 44(6):627–631
10. Cassayre L, Chamelot P, Arurault L, Massot L, Palau P, Taxil P (2007) Corros Sci 49:3610–3625
11. Yang J, Hryn JN, Krumdick GK (2006) In: Galloway TJ (ed) Light Metals. TMS, Warrendale, pp 421–424
12. Apisarov A, Dedyukhin A, Nikolaeva E, Tinghaev P, Tkacheva O, Redkin A, Zaikov Y (2011) Metall Mater Trans B 42:236–242
13. Apisarov AP, Dedyukhin AE, Red'kin AA, Tkacheva OY, Zaikov YP (2010) Russ J Electrochem (Engl Transl) 46(6):633–639
14. Zajkov JP, Suzdal'tsev AV, Khramov AP, Kovrov VA (2007) Pat. RU2368707C2
15. Wagman DD, Evans WH, Parker VB et al (1982) The NBS tables of chemical thermodynamic properties. J Phys Chem Ref Data 11(Suppl 2):399
16. Glushko VP (ed) (1978–1982) Thermodynamic properties of individual substances, vol 1–4. Science Press, Moscow